



OPEN

SUBJECT AREAS:
CANCER THERAPY
DRUG DISCOVERY
CHEMICAL SYNTHESIS
CELL DEATHReceived
29 January 2014Accepted
1 May 2014Published
21 May 2014Correspondence and
requests for materials
should be addressed to
J.W.S. (shaojingwei@
fzu.edu.cn) or L.J.
(pharmlink@gmail.
com)* These authors
contributed equally to
this work.

Synergism of ursolic acid derivative US597 with 2-deoxy-D-glucose to preferentially induce tumor cell death by dual-targeting of apoptosis and glycolysis

Jichuang Wang^{1*}, Zhou Jiang^{1*}, Liping Xiang¹, Yuanfang Li¹, Minrui Ou¹, Xiang Yang¹, Jingwei Shao¹, Yusheng Lu¹, Lifeng Lin¹, Jianzhong Chen², Yun Dai³ & Lee Jia¹¹Cancer Metastasis Alert and Prevention Center, College of Chemistry, Fuzhou University, 523 Industry Road, Science Building, 3FL., Fuzhou, Fujian 350002, China, ²School of Pharmacy, Fujian University of Traditional Chinese Medicine, Fuzhou, Fujian 350108, China, ³Virginia Commonwealth University and the Massey Cancer Center, Room 234 Goodwin Research Building, 401 College Street, Richmond VA 23298, USA.

Ursolic acid (UA) is a naturally bioactive product that exhibits potential anticancer effects. The relatively safe and effective molecule intrigued us to explore a way to further improve its anti-cancer activity and tumor-targeting specificity. In the present study, a series of structural modifications of UA was achieved, which resulted in significant increase in growth inhibition on various cancer cell lines with minimal effects on normal cells. The leading molecule US597 (UA-4) caused depolarization of mitochondrial membrane potential, cell arrest in G0/G1 phase and apoptosis/necrosis in a dose-dependent manner. Structural docking suggested that the carbon chains of the modified UA derivatives compete strongly with glucose for binding to glucokinase, the key glycolysis enzyme presumably active in cancer cells. The combination of 2-deoxy-D-glucose (2-DG) and UA-4 induced cell cycle arrest in G2/M phase, promoted caspase-dependent cell death, reduced hexokinase activity, aggravated depletion of intracellular ATP, decreased lactate production and synergistically inhibited cancer cell growth *in vitro* (HepG2) and *in vivo* (H22). Collectively, our findings suggest that the structural modification enhances efficacy and selectivity of UA, and the combination of UA-4 with 2-DG produces synergistic inhibition on hepatoma cell proliferation by dual targeting of apoptosis and glycolysis.

Ursolic acid (UA, 3 β -hydroxy-urs-12-en-28-oic acid) is a natural pentacyclic triterpenoid carboxylic acid that represents one of the major components of some traditional medicinal herbs. UA exhibits a wide range of biological functions, such as anti-inflammatory¹⁻³, anti-diabetic^{4,5}, anti-HIV⁶⁻⁹, anti-oxidative¹⁰ and antimalarial activities¹¹. Among them, its anti-cancer activity is the most prominent in both the *in vitro* and *in vivo* settings¹²⁻¹⁷.

In recent years, many attempts on structural modifications of UA have been made to improve its efficacy and specificity against cancer cells¹⁸⁻²¹. Modifications of UA have been mainly focused on its 3-OH and 17-COOH functional groups. Introduction of polar groups or active groups to the main structure may significantly improve anti-cancer activity and water solubility of UA derivatives^{22,23}. For example, introduction of an acetyl group and amino alkyl group into the 3-OH and the 17-COOH positions remarkably improves UA's activity in inhibition of cell proliferation^{24,25}. We previously reported an approach by which diethanol amine was connected to UA after chlorinating 17-COOH group with oxalyl chloride. Such a derivative displayed better anti-proliferative activity against human cancer cells (e.g., HepG2, BGC-823, SH-SY5Y and HeLa)²⁶, suggesting that this modification improves the anticancer efficacy of UA derivatives. However, the majority of UA derivatives do not possess tumor targeting ability and have greater toxicity on normal tissues, which limit their further development and application.



The therapeutic targeting of cancer metabolism has become a novel strategy of drug development²⁷. Cellular metabolism of tumor cells differs significantly from that of normal cells. Cancer cells have defective mitochondria, which forces them to mainly depend on anaerobic glycolysis for production of lactate and ATP as their main source of energy even in the presence of sufficient oxygen. This is known as Warburg's effect in cancer cells²⁸. Selectively targeting cancer metabolism may provide an alternative strategy for anticancer drug development with minimum adverse effects on normal cells²⁹.

2-Deoxy-D-glucose (2-DG) is a glucose analog that is best known as an inhibitor of glucose metabolism³⁰. 2-DG blocks the first step of glycolysis. It is phosphorylated by hexokinase II and this phosphorylated product 2-deoxyglucose 6-phosphate (2-DG-6P) cannot be further metabolized. Many cancers have elevated glucose uptake and hexokinase levels, and thus 2-DG has been suggested as a molecular cancer therapeutic based on its actions as a competitive inhibitor of glucose transporters, hexokinase, and glycolysis in cancer cells³¹. Whereas 2-DG ultimately suppresses cell proliferation *in vitro*^{32,33}, animal model studies and human clinical trials indicate that 2-DG treatment, when provided as a single agent, scarcely inhibits tumor growth^{34,35}.

In the present study, we synthesized a series of UA diamine derivatives, and tested their selectivity and efficacy on various cancer cell lines versus their counterpart normal cells. Moreover, led by the results from our computational docking study, we tested whether combination of the identified leading UA derivative US597 (UA-4) and 2-DG could result in synergistic inhibition on hepatoma cell proliferation *in vitro* and *in vivo*, and further explored the potential mechanisms of the combined actions.

Results

Chemistry of UA derivatives. UA was acetylated to give 3-O-acetylursolic acid (UA-1). Treatment of 3-O-acetylursolic acid with oxalyl chloride yielded 28-acylchloride, which was further combined with di-amine to yield the di-amine UA derivatives UA-2 ~ UA-5 (Fig. 1). The characterization data of 3 β -acetoxy-urs-12-en-28-oic acid hexamethylenediamine (UA-4) were as follows: yield: 80.1%; mp: 103–105°C; IR (KBr) ν : 3368, 2926, 1734, 1646, 1524, 1456, 1372, 1248, 1028 cm^{-1} ; $^1\text{H-NMR}$ (500 MHz, CDCl_3) δ : 5.95 (t, $J = 5.0$ Hz, 1 H, CONHCH₂), 5.30 (t, $J = 3.5$ Hz, 1 H, H-12), 4.49 (dd, $J = 5.0, 6.0$ Hz, 1 H, H-3), 3.33 (dt, $J = 7.0, 6.5$ Hz, 2 H, NHCH₂CH₂), 2.98

(m, 2 H, CH₂CH₂NH₂), 2.83 (d, $J = 3.5$ Hz, 1 H, H-18), 2.05 (s, 3 H, CH₃COO), 1.09 (s, 3 H, CH₃), 0.97–0.93 (m, 6 H, 2 \times CH₃), 0.89–0.84 (m, 9 H, 3 \times CH₃), 0.78 (s, 3 H, CH₃); ESI-MS m/z : 597.5 (M + H)⁺ (Supplementary Fig. S1). Characterization data of UA-2, UA-3 and UA-5 were shown in Supplementary Information (SI).

Saponification of UA-2 ~ UA-5 produced compounds UA-6 ~ UA-9, respectively (Fig. 1). The characterization data of N-[3 β -hydroxy-urs-12-en-28-oyl]-amino-hexamethylenediamine (UA-8) were as follows: yield: 79.6%; mp: 202–204°C; IR (KBr) ν : 3398, 2928, 1640, 1530, 1454, 1376, 1046, 996 cm^{-1} ; $^1\text{H-NMR}$ (500 MHz, CDCl_3) δ : 8.36 (s, 1 H, OH), 6.05 (t, $J = 5.5$ Hz, 1 H, CONHCH₂), 5.31 (t, $J = 4.5$ Hz, 1 H, H-12), 3.33 (m, 2 H, NHCH₂CH₂), 3.22 (dd, $J = 4.5, 5.0$ Hz, 1 H, H-3), 3.01 (m, 2 H, CH₂CH₂NH₂), 2.96 (d, $J = 5.0$ Hz, 1 H, H-18), 1.09 (s, 3 H, CH₃), 0.99 (s, 3 H, CH₃), 0.96–0.91 (m, 6 H, 2 \times CH₃), 0.87 (d, $J = 6.5$ Hz, 3 H, CH₃), 0.79 (s, 3 H, CH₃), 0.80–0.75 (m, 6 H, 2 \times CH₃); ESI-MS m/z : 555.9 (M + H)⁺. Characterization data of UA-6, UA-7 and UA-9 were showed in Supplementary Information.

The purity of UA-4 was determined by using the established HPLC method. In each single run, only a major peak was observed, which dominated the chromatographic area, indicating that UA-4 has the purity >98%. The retention time of UA-4 was at 9.21 min (Supplementary Fig. S1).

Inhibition potency of UA derivatives. The inhibition potency of all the synthesized UA derivatives was tested by using different cancer cell lines HepG2, AGS, A-375, HeLa, and human normal counterpart cell line HELF. The results were compared and ranked. As shown in Table 1 and Supplementary Fig. S2b, the IC₅₀ values for UA to suppress cell proliferation varied from 33.12 ~ 68.82 μM in four cancer cell lines. The 3-OH of the modified UA derivatives was esterified, which resulted in 3-O-acetyl UA (UA-1). UA-1 showed inhibition activity similar to UA itself against the HepG2, AGS, A-375, and HeLa cell lines, while UA-1 had lower cytotoxicity against HELF cells than UA. In addition, most of the UA derivatives, such as UA-2 ~ UA-9, exhibited an increased cytotoxic activity in various degree compared with UA. Derivatives UA-2 ~ UA-5 with an acetoxy group exhibited cytotoxicity against A-375 and HeLa cells more potent than UA-6 ~ UA-9, the latter had a free 3-hydroxyl group (Supplementary Fig. S2a and b). The result showed the difference in potency between acetoxy and hydroxyl groups

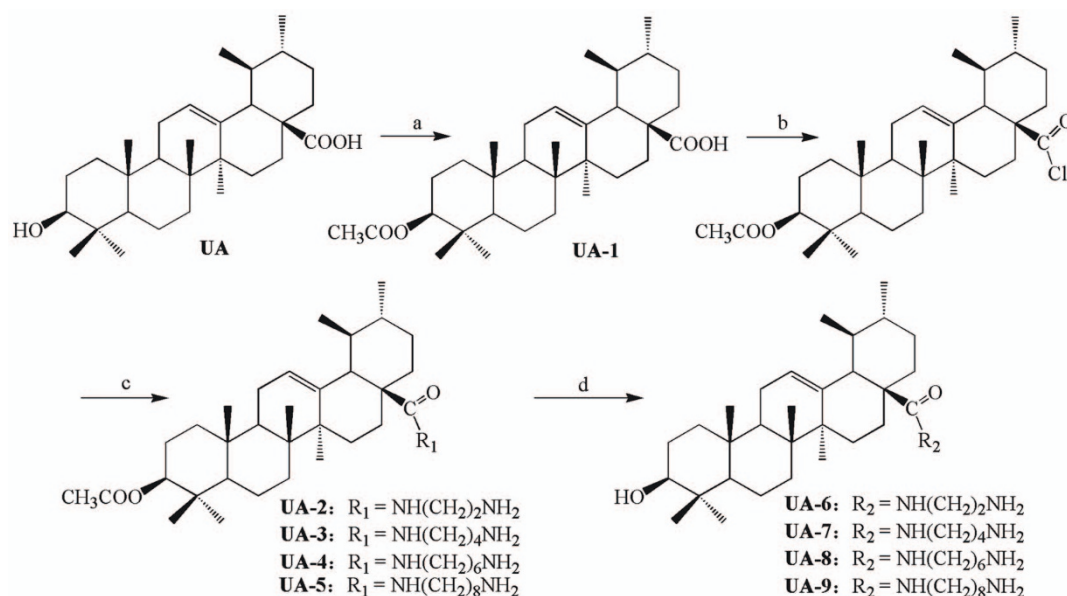


Figure 1 | Synthesis of di-amine derivatives of UA. Reagents and conditions include (a) anhydride/pyr/DMAP, R.T.; (b) (CO)₂Cl, CH₂Cl₂, R.T.; (c) di-amine, CH₂Cl₂, R.T.; and (d) NaOH, CH₃OH/THF, R.T.

Table 1 | *In vitro* activity of UA, its derivatives UA-1 ~ UA-9, and paclitaxel on human tumor cells vs. normal cell lines

Compound	IC50 (μM) ^a				
	HepG2	AGS	A-375	HeLa	HELF
UA	68.82 ± 3.71	43.25 ± 2.13	57.55 ± 3.21	33.12 ± 0.63	21.28 ± 1.76
UA-1	71.26 ± 2.18	42.88 ± 1.22	50.89 ± 1.79	26.09 ± 1.99	54.53 ± 2.01**
UA-2	16.32 ± 1.76**	14.51 ± 0.85**	4.15 ± 0.98**	4.37 ± 2.51**	18.08 ± 2.05
UA-3	15.97 ± 2.18**	14.07 ± 1.37**	4.07 ± 1.22**	4.19 ± 2.86**	25.11 ± 2.86
UA-4	7.20 ± 2.04**	12.84 ± 2.15**	3.86 ± 1.52**	3.79 ± 3.14**	14.9 ± 2.81*
UA-5	17.34 ± 2.53**	— ^b	5.06 ± 1.26**	8.56 ± 0.12*	36.05 ± 1.82**
UA-6	13.9 ± 0.78**	17.72 ± 2.31**	13.63 ± 2.39**	14.56 ± 1.12**	15.43 ± 2.37
UA-7	14.44 ± 1.38**	17.48 ± 1.64**	15.07 ± 1.47**	14.45 ± 2.65**	15.01 ± 1.89
UA-8	13.42 ± 2.31**	16.56 ± 1.80**	11.9 ± 1.33**	13.27 ± 0.87**	12.37 ± 0.69*
UA-9	26.65 ± 1.403*	— ^b	16.40 ± 0.87**	16.90 ± 1.69*	39.40 ± 1.43
Paclitaxel	10.32 ± 0.02**	9.24 ± 0.13**	8.56 ± 0.07**	6.62 ± 0.21**	7.17 ± 0.08*

^aDrug concentration that inhibits cell growth by 50%.
^bNo data were recorded by “—”.
 Data represents mean ± SD (n = 6).
 *P < 0.05;
 **P < 0.01 compared to the vehicle-treated control.

(Supplementary Fig. S2), and suggested that the acetoxyl group may be more potent than hydroxyl group in inhibiting cell growth. After careful analysis of the data, we noted that UA-4 showed the most significant activity against all cancer cell lines (i.e., HepG2, AGS, A-375, and HeLa) but less cytotoxicity towards the normal counterpart HELF cells in comparison to the positive control drug paclitaxel (Table 1, Supplementary Fig. S2). Based on the comparison and evaluation of potency and selectivity of the UA derivatives on the tested cell lines, UA-4 was then chosen for further studies to explore its antitumor mechanism.

Effects of UA-4 on cell cycle distribution. Based on the above-obtained data, we decided to explore the cellular mechanism by which UA-4 affects cell cycle distribution. A-375 cells were treated with different concentrations of UA-4. The cell cycle was then analyzed by flow cytometry after the cells were stained for DNA with PI. When the number of cells in S and G2/M phases was reduced, the number of those in G₀/G₁ phase was increased gradually with increasing concentrations of UA-4, (Fig. 2c), indicating that UA-4 arrests A-375 cells in G₀/G₁ phase.

UA-4 induced loss of $\Delta\Psi\text{m}$. Mitochondrial membrane depolarization is a prelude of apoptosis. $\Delta\Psi\text{m}$ reflects activity of electron transport chain and thus mitochondrial function. After A-375 cells were treated with UA-4, the loss of $\Delta\Psi\text{m}$ was observed in a dose-dependent manner (Fig. 2d). The loss of $\Delta\Psi\text{m}$ occurred at 1 μM of UA-4 (106% of Rhodamine⁺ cells, compared to the untreated control) and reached the maximum at 10 μM (132% of Rhodamine⁺ cells).

UA-4 induced apoptosis/necrosis. To determine whether induction of apoptosis/necrosis by UA-4 contributes to its anti-cancer activity of UA derivatives, Annexin V-FITC/PI double staining kit was used to analyze apoptosis/necrosis in A-375 cells after the cells were treated with different concentrations of UA-4. The representative results of three independent experiments were shown in Fig. 2e and f. Different states of cell death were defined as follows: healthy cells are localized in the lower-left quadrant (Annexin V⁻/PI⁻); early apoptotic cells in the lower-right quadrant (Annexin V⁺/PI⁻); late apoptotic cells and necrotic cells in the upper-right quadrant (Annexin V⁺/PI⁺); and necrotic cells in the upper-left quadrant (Annexin V⁻/PI⁺). As shown in Fig. 2e and f, exposure to UA-4 for 12 h and 24 h, the proportion of annexin-V⁺/PI⁺ cells were evidently increased in a time- and dose-dependent manner, while there was little increase in the number of annexin-V⁺/PI⁻ cells,

suggesting an increase in the number of necrotic cells. Combined with the result of TUNEL assay (Fig. 2g), the proportion of annexin-V⁺/PI⁺ cells had both late apoptotic and necrotic cells. Through comparative analysis, the decrease in cell viability induced by UA-4 was not entirely attributed to necrosis/apoptosis (Fig. 2b, 2e and 2f), and we hypothesized that it might be associated with changes in cellular energy metabolism.

Computational modeling to predict binding of 2-DG and UA derivatives to glucokinase for synergistic inhibition. To confirm our hypothesis that the cell death was related to cancer cell cellular energy metabolism, we further performed computational modeling analysis. After ranking the potency order of the UA derivatives and identifying the leading molecules, we established a computational docking model to explore whether UA derivatives (UA-2 ~ UA-9) could directly affect glucokinase activity and whether the synergistic inhibition existed between 2-DG and UA derivatives. The crystal structure of glucokinase from *Homo Sapiens* had been reported³⁶. The chemical structures of 2-DG, glucose (Glc) and UA derivatives UA-2 ~ UA-9 were shown in Supplementary Fig. S3. The docked complex structure constituted glucokinase and one of the carbon chain fragments of different length, simply named as 2C, 4C, 6C and 8C, respectively, as shown in Fig. 3 and Supplementary Figs. S4–S5. UA itself has difficulty to be docked in glucokinase. There are two glucose binding sites in glucokinase (Supplementary Fig. S4a)³⁷. The relative binding energy of glucose to the two different sites was -157.79 KJ/mol (Supplementary Figs. S4b and 5a, Site 1), and -158.89 KJ/mol (Supplementary Figs. S4d and 5c, Site 2), respectively. The docked structure showed that glucose had similar affinity to the two active sites of glucokinase. Fragment 2C could bind to active site 1 of glucokinase with relative binding energy -84.60 KJ/mol (Supplementary Figs. S4b and 5b). 2-DG could bind to active site 2 of glucokinase (Fig. 3a and Supplementary Figs. S4c, 4d and 5d). Fig. 3 shows that fragments 4C, 6C, and 8C could bind to active site 2 of glucokinase with the relative binding energy -109.93, -133.02 and -146.28 KJ/mol, respectively. The binding sites of the fragments are the same as those of 2-DG and glucose binding site 2 (Supplementary Figs. S4c and 4d). Fragment 6C of UA-4 and UA-8 showed the strongest binding affinity to glucokinase, and it competed well with glucose for the active sites of glucokinase. The docking data demonstrated that UA-4 was the best candidate for potential targeting cancer cell glycolysis metabolism, which was well consistent with our MTT and Annexin V-FITC/PI staining result *in vitro*.

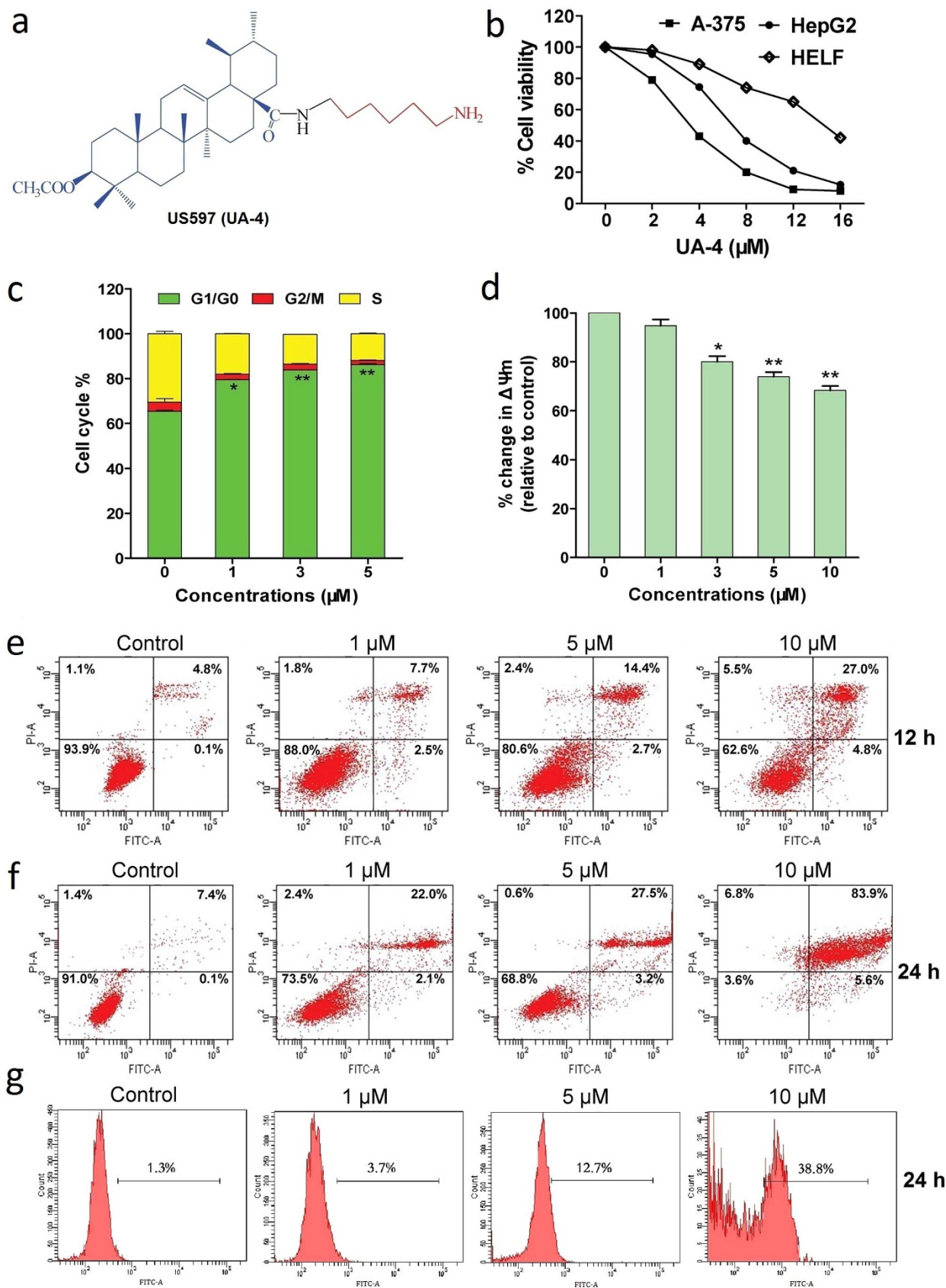


Figure 2 | Structure and pharmacological effects of UA-4. a, the structural formula of UA-4; b, dose-response of anti-proliferative effect of UA-4 on A-375, HepG2 and HELF cells; c, effects of UA-4 on cell cycle distribution in A-375 cells; d, effects of UA-4 on $\Delta\Psi_m$ in A-375 cells. Results are expressed as percentage change in UA-4 treatment compared to the vehicle-treated control (* $P < 0.05$, ** $P < 0.01$). e, A-375 cells were treated with UA-4 (1, 5, 10 μM) for 12 h, and 24 h (f), respectively. Apoptosis was determined by Annexin-V-FITC/PI labeling. g, One step TUNEL apoptosis was tested on A-375 cells treated with UA-4 (1, 5, 10 μM) for 24 h.

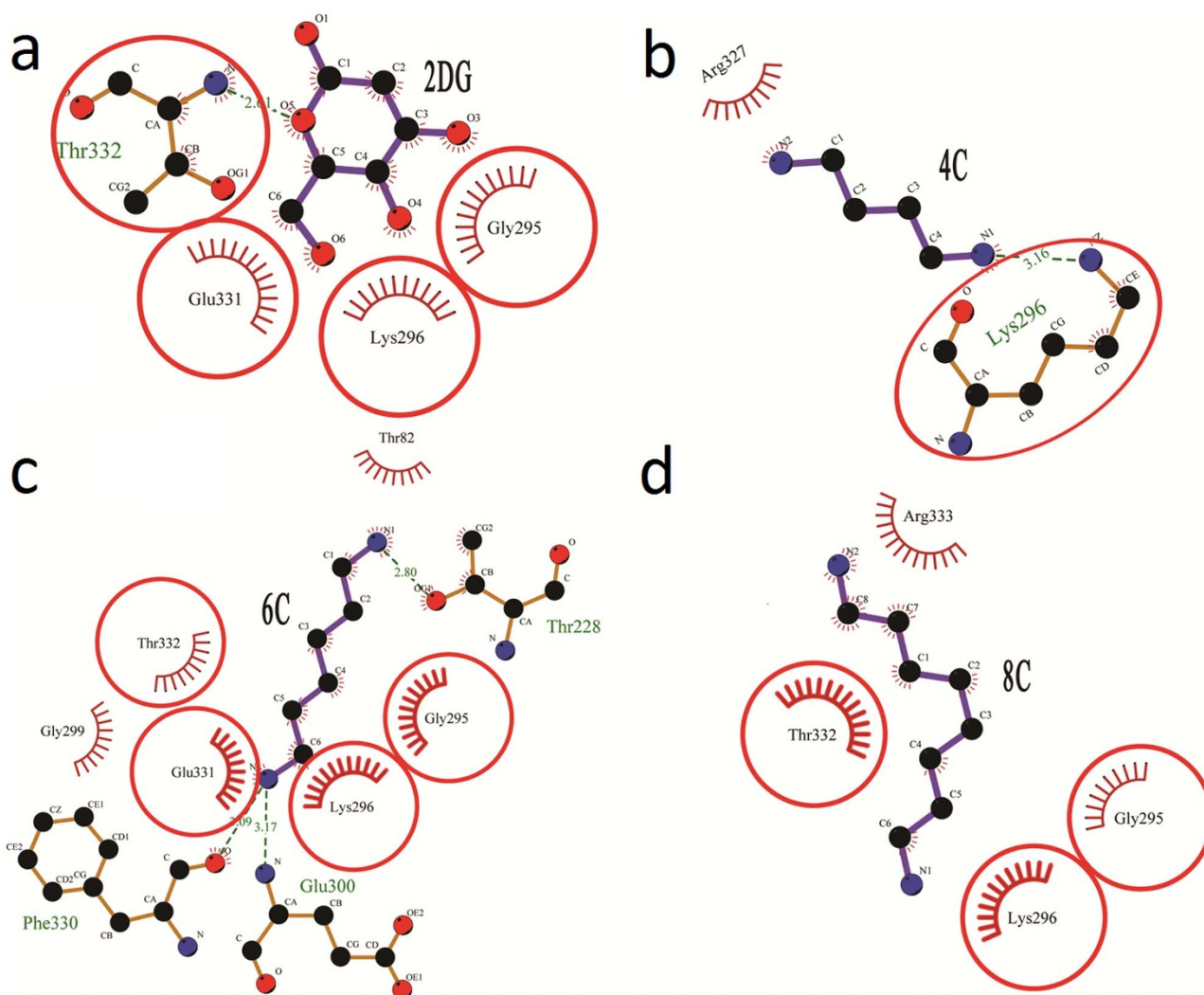


Figure 3 | The binding simulation between hexokinase and 2-DG, 4C, 6C and 8C of the UA derivatives. a, 2-DG binds with amino acid residues Glu 331, Lys 296 and Gly 295 of hexokinase via hydrophobic interaction, and binds with Thr 332 via hydrogen bonds; b, 4C binds with amino acid residue Lys 296 as 2-DG binds to one of the four residues of hexokinase; c, the docking and binding between 6C of UA-4 or UA-8 and hexokinase are the same as those between 2-DG and hexokinase. Furthermore, 6C can bind the amino acid residues Phe 330, Glu 300 and Thr 228 via hydrogen bond, the reaction that could not be simulated between 2-DG and hexokinase. d, 8C binds with amino acid residues Thr 332, Gly 295, and Lys 296 via hydrophobic interaction.

The combination of 2-DG and UA-4 synergistically inhibits cancer cell growth *in vitro*. To further examine the synergistic effect existing between UA-4 and glycolytic inhibitors, L-Cys, 2-DG, LM and 3-BrPA were combined with UA-4, respectively. Comprehensively considering the high inhibition of cancer cell proliferation and low-toxicity to normal cells, the combination of 2-DG and UA-4 proved the best combination (Fig. 4a and b).

Lastly, we investigated effects of UA-4 alone, 2-DG alone or combination on proliferation of cancer A-375, cancer HepG2, normal HELF and normal L02 cells. As showed in Fig. 4c, 4d and Supplementary Fig. S6, the combination of the two drugs produced significant inhibition on cancer cell lines A-375 and HepG2 in a dose-dependent manner in comparison with either 2-DG or UA-4 treatment alone (Fig. 4c and Supplementary Fig. S6a). Whereas, the combination did not produce significant inhibition on the human normal cell lines HELF and L02 in comparison with either 2-DG or UA-4 treatment alone (Fig. 4d and Supplementary Fig. S6b). In order to investigate the mechanism of cell death promoted by the 2DG/UA-4 combination, we selected the HepG2 cell line for further study because of better combination effects.

The combination of 2-DG and UA-4 induces cell cycle arrest in G2/M phase. Because the decrease in cell viability induced by UA-4 was not entirely attributed to necrosis/apoptosis (Fig. 2e and 2f), we asked whether cell cycle was affected by 2-DG + UA-4. HepG2 cells were treated for 24 h in the presence of UA-4 or/and 2-DG. 2-DG alone led to a cell cycle arrest in G2/M, while UA-4 alone arrested cell cycle at G0/G1 stage (Figs. 2c and 5a). Interestingly, the combination of UA-4 (4 μ M) and 2-DG (20 mM) led to the accumulation of 37.1% HepG2 arrested in G2/M stage (Fig. 5a). The results showed the combination of 2-DG and UA-4 could arrest cell cycle in G2/M phase.

The combination of 2-DG and UA-4 promotes caspase-dependent cell death. To determine if the inhibition of cancer cell proliferation by the combination of the drugs is due to apoptosis, we analyzed Annexin V-FITC/PI double staining in HepG2 cells. As shown in Fig. 5b, the combination of 2-DG and UA-4 significantly increased apoptosis (31.2%), compared with the single drug (13.7% and 24.7%). The caspase cascade is crucial for apoptotic signal transduction³⁸. Activities of caspase-3, caspase-8 and caspase-9 were shown to

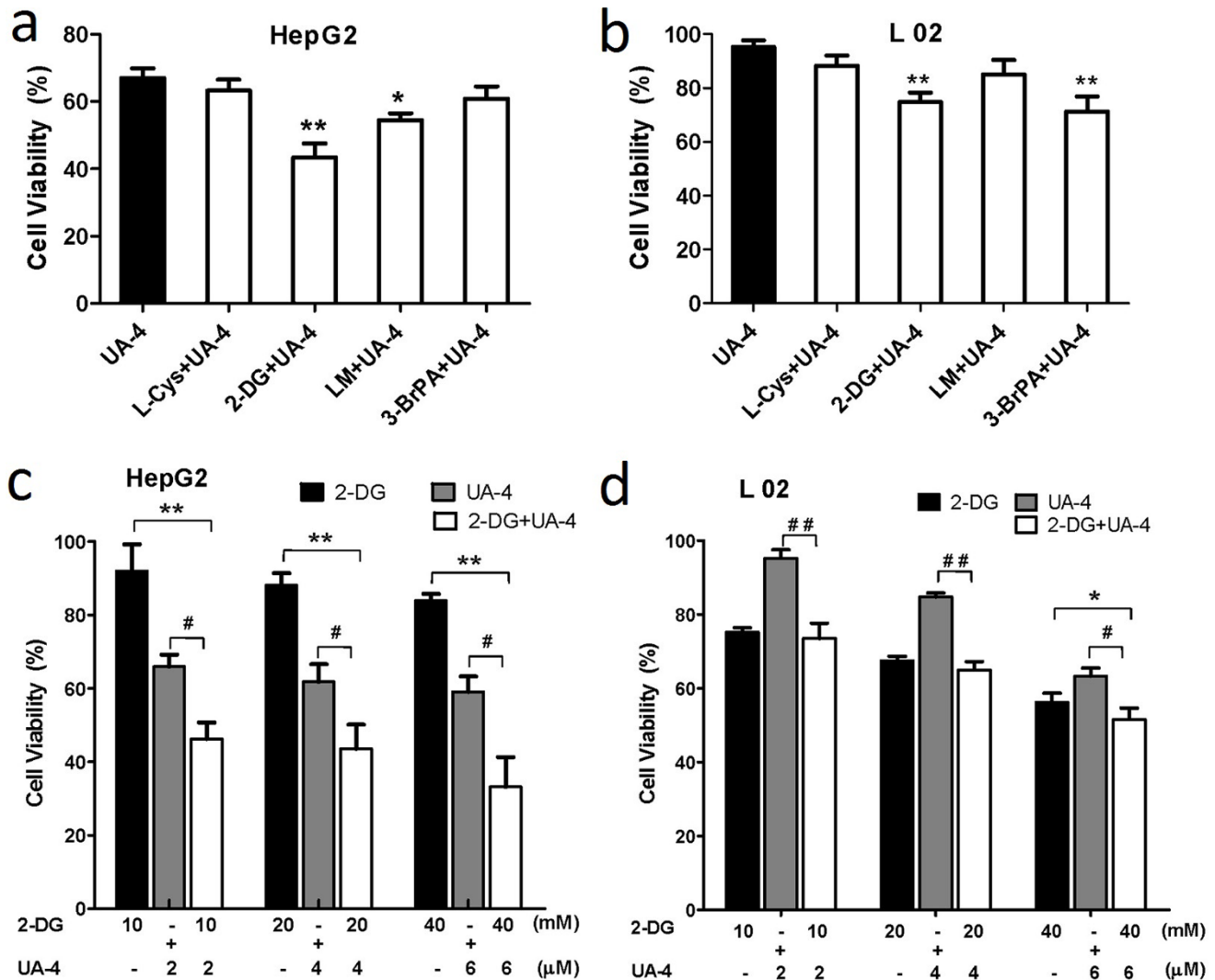


Figure 4 | UA-4 elicited synergistic inhibition on cancer cells with glycolysis inhibitors and affects HepG2 cancer cell metabolism induced by 2-DG. HepG2 (a) and L02 (b) cells were treated for 24 h with UA-4 at 4 μM and four glycolysis inhibitors (L-Cys: 15 mM; 2-DG: 50 mM; LM: 2.5 mM and 3-BrPA: 64 mM) at IC₈₀. HepG2 (c) and L02 (d) cells were treated with compound UA-4 in the presence and absence of 2-DG followed by cell viability assay (**p* < 0.05, ***p* < 0.01, #*p* < 0.05 and ##*p* < 0.01, compared to the combination groups).

be dose-dependently increased with treatment of 2-DG, UA-4 and 2-DG + UA-4 for 24 h in HepG2 cells (Fig. 5c–5e). The results showed the combination of 2-DG and UA-4 could promote caspase-dependent apoptosis.

The combination of 2-DG and UA-4 reduces hexokinase activity. To verify whether the combination of UA-4 and 2-DG have direct inhibition effect on the hexokinase activity in HepG2 cells, the total hexokinase (HK) activity in the presence of UA-4 and/or 2-DG were measured. The results demonstrated that single drug UA-4 or 2-DG could reduce the activity of hexokinase on different levels, but the combination of UA-4 and 2-DG synergistically inhibited HK activity (Fig. 5f).

The combination of 2-DG and UA-4 aggravates depletion of intracellular ATP. We determined whether the combination of 2-DG and UA-4 affects intracellular ATP levels in HepG2 cells (Fig. 5g). 2-DG alone slightly decreased intracellular ATP concentrations with 24 h of treatment. UA-4 also decreased intracellular ATP concentration in a concentration-dependent manner. Importantly, the combination of 2-DG and UA-4 robustly diminished intracellular ATP concentrations in HepG2 cells. These results suggested

that the combination of 2-DG and UA-4 could exert a more deleterious effect on cancer cell viability by aggravating intracellular ATP depletion.

The combination of 2-DG and UA-4 decreases lactate production. To elucidate if the combination of UA-4 and 2-DG could affect cancer cell metabolism, the lactate production in the tumor cells was tested. 2-DG decreased lactate production and prevented UA-4 induced lactate production in HepG2 cancer cells (Fig. 5h). In conclusion, these results suggest the synergistic inhibition of the combination on HepG2 cancer cells, probably reflecting the inhibition by 2-DG on cellular glycolysis that is dominant in most malignant cancer cells.

Calculation of synergism for the combination of 2-DG and UA-4. The *q* values for quantification of synergism and antagonism were calculated for cytotoxicity, hexokinase activity, ATP level and lactate production. By calculation method of Zheng-jun Jin³⁹, the combination of 2-DG and UA-4 had synergism for cytotoxicity (*q* ≥ 1.15), and had additive effect (0.85 < *q* < 1.15) for lactate production. However, the combination of 2-DG and UA-4 at low concentrations had synergism for hexokinase activity and the ATP

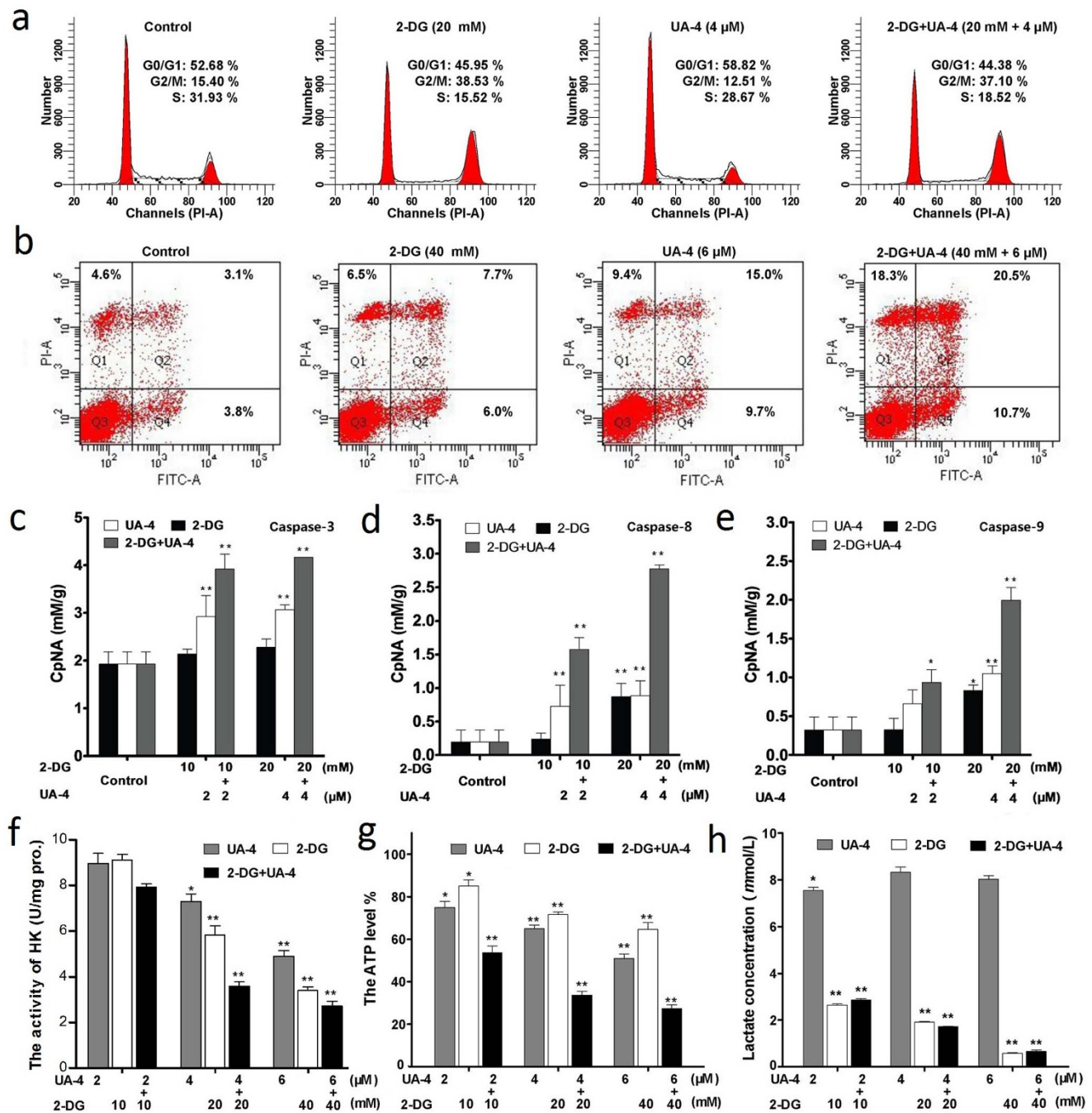


Figure 5 | The mechanism of anti-proliferation by the combination of UA-4 and 2-DG in HepG2 cells. HepG2 cells were treated with 2-DG, UA-4 and 2-DG + UA-4 for 24 h. The cell cycle stages (a) and apoptosis (b) were determined by flow cytometry analysis. The activities of caspase (c, d, e), hexokinase activity (f) and ATP level (g) were determined by microplate reader, and lactate concentrations in medium (h) were detected by lactate assay kit (* $p < 0.05$, ** $p < 0.01$, compared to the control group).

level, and had additive effect at high concentration (Supplementary Table S1). Thus, the combination of 2-DG and UA-4 was synergistic to inhibit cancer cell growth *in vitro*, reduce hexokinase activity, aggravate depletion of intracellular ATP and additive to decrease lactate production.

The combination of 2-DG and UA-4 synergistically inhibits tumor growth *in vivo*. Our aforementioned results showed that the combination of 2-DG and UA-4 synergistically inhibited the growth of both HepG2 and A-375 cells *in vitro* (Fig. 4c–4d and Supplementary Fig. S6). Our data (Supplementary Fig. S7) showed that both UA-4 single agent or combined with 2-DG were more

sensitive to H22 cells than to HepG2 cells. To confirm these results *in vivo*, we tested the combined treatment of 2-DG and UA-4 in a H22 cells-bearing ascites mice model. During 14 days of drug treatment, the tumor volume in each experimental group increased (Fig. 6a, upper and 6b), while body weight of mice had no significant changes (Fig. 6c). The combination of 2-DG and UA-4 significantly inhibited tumor growth in a dose- and time-dependent manner, compared with the single-drug group and control group (Fig. 6b). At 14 days, normal tissues, such as heart, liver, spleen, lung, kidney and small intestine, did not exhibit significant morphological changes by a histological analysis of the tissue (Supplementary Fig. S8). The tumor inhibition rate was calculated

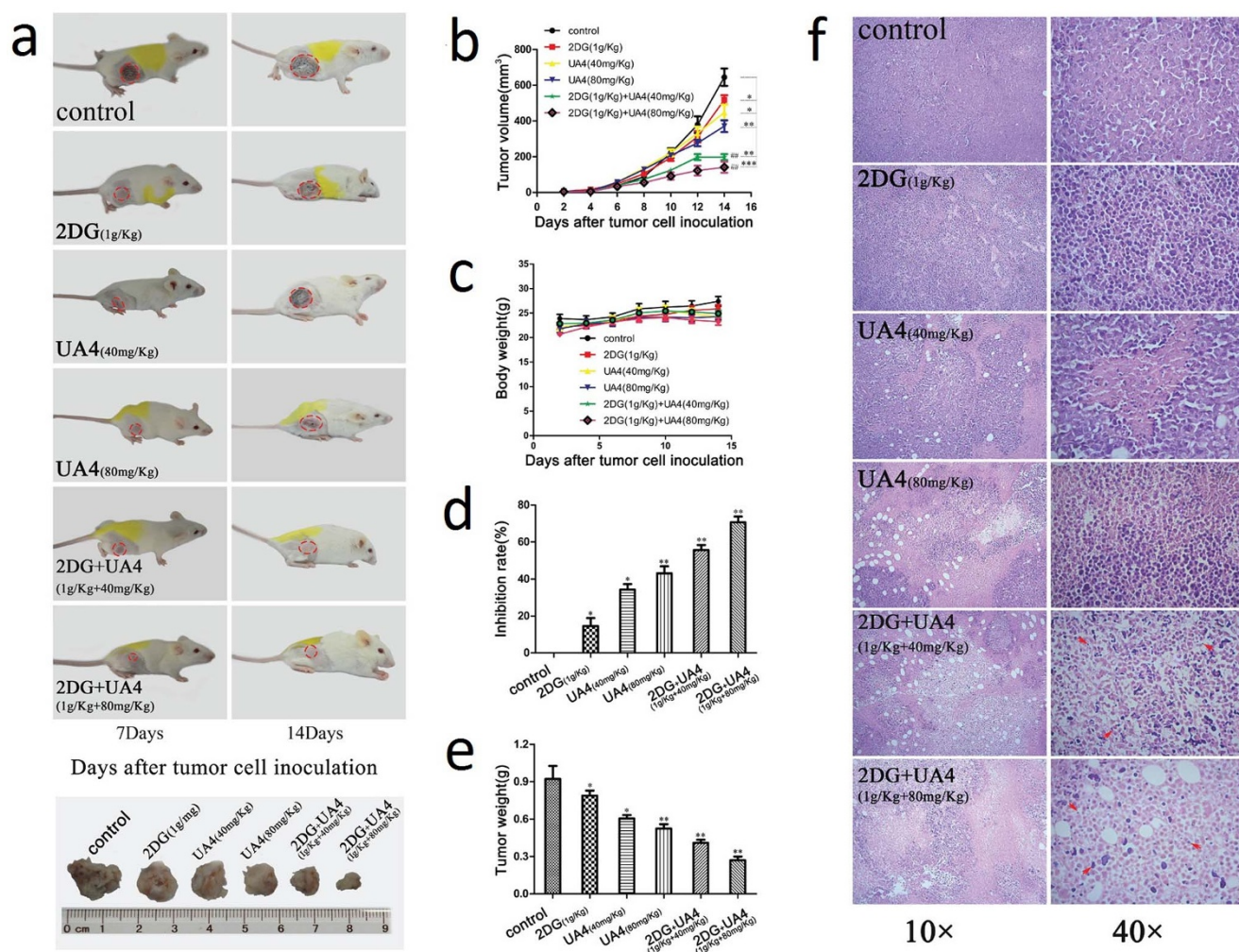


Figure 6 | The combination of 2-DG and UA-4 effectively inhibits tumor growth in H22 tumor-bearing mice. a, photographs of vehicle-treated or drug-treated H22 tumor-bearing mice with representative tumors. Photographs were taken at 7 and 14 days after compounds treatment. The bottom images show tumor volume of the groups at 14 days. Tumor volume (b) and mice weight (c) were measured every other day. After 14 days, inhibition rate (d) and tumor weight (e) were quantitatively analyzed. f, histological examinations; tumors were analyzed by hematoxylin and eosin staining for histological features. (* $p < 0.05$, ** $p < 0.01$, compared to the control group).

from a qualitative/quantitative statistical analysis of tumor volume and weight (Fig. 6a bottom and Fig. 6d–6e). Among them, the tumor inhibition rate of 2-DG + UA-4 (1 g/Kg + 80 mg/Kg) was up to $70.2 \pm 3.4\%$, compared with the control group. Histological examinations showed great tumor necrosis and apoptosis (arrows) appeared in the combination group of 2-DG and UA-4 (Fig. 6f).

Discussion

Our previous study showed significant improvement on inhibition by UA of cancer cell growth after introduction of both the acetyl group and amino alkyl group to the 3-COOH position and 17-OH position of UA, respectively²⁶. In the present study, we observed modest changes in IC_{50} values of the UA derivatives after the 3-OH group was acetylated alone (e.g., UA-1, Table 1). However, significant improvement on inhibition of cell growth was achieved when both the acetyl group and diamine group with different length of carbon chains (2C, 4C, 6C and 8C) were introduced to the 3-OH and the 17-COOH positions, respectively (e.g., compounds UA-2 ~ UA-5). Interestingly, in most of the tested cancer cell lines (except HepG2), the potency of compounds UA-2 ~ UA-5 (with both acetyl and diamine groups) was higher than their corresponding analogs (UA-6 ~ UA-9). The latter had a free unmodified 3-OH group. The result supports our hypothesis that concurrent modification at the

3-OH and 17-COOH positions of UA with the acetyl and diamine groups could improve the inhibition potency of UA.

The inhibitory effect of the UA diamine derivatives (UA-2 ~ UA-5) on cancer cells varied when the length of the carbon chain was changed. In the process of structural and functional optimization for the activity of the UA derivatives to compete with the substrates of hexokinase (i.e., glucose), UA-4 displayed the most significant anti-proliferation effect against various cancer cell lines (Table 1). We proposed that the length of six carbon chain (6C) may represent the most optimal length for UA-4 to bind the active sites of hexokinase when competing with the six carbon glucose (Fig. 3 and Supplementary Fig. S4) to produce inhibition of the key enzyme in the glycolysis pathway, and hence down-regulate the glycolysis metabolism of cancer cells. Cancer cells may contain higher levels of esterase and amidase than normal cells¹⁸. We hypothesized that once endocytosed, UA-4 may be hydrolyzed by amidase to produce the metabolized products 6C and UA, respectively. As showed by the computational simulation (Fig. 3), 6C docked well with the active sites of hexokinase to compete with glucose, and therefore resulting in binding and inhibiting the rate-limiting enzyme—hexokinase in cancer cells. In the mean time, the hydrolyzed UA itself possesses the ability to induce cell apoptosis, inhibit cell proliferation and arrest cell cycle as previously revealed by us and others^{12,15,16,26}. These joint effects of UA-4, resulted from



its hydrolyzed parts UA and 6C together, are depicted and summarized by us in Fig. 7, which represents the mechanism of action by which UA-4 exhibits its anti-cancer activity.

Cancer cells are sensitive and vulnerable to biological changes under hypoxic conditions that would sensitize cancer cells to glucose changes in cell microenvironment. One of the fundamental changes that occurs in most cancer cells is the shift in energy metabolism from oxidative phosphorylation to aerobic glycolysis to compensate bioenergy ATP. The present study demonstrated that UA-4 produced mitochondrial membrane depolarization of cancer cells dose-dependently (Fig. 2d), suggesting that UA-4 may be a mitochondrial inhibitor. The finding intrigued us to explore a combined inhibition of glycolysis and mitochondrial function by concomitantly adding 2-DG and UA-4 to A-375 and HepG2 cells. The present studies observed the clear synergistic effect between UA-4 and 2-DG in inhibiting cancer cell activity. 2-DG is the most commonly-used antiglycolytic agent^{40–42}. In the present study, we found that UA-4 primarily arrested cancer cells in G0/G1 phase. While in its combination with 2-DG, the cells were dominantly arrested in G2/M stage. The combination elicited cytotoxic effect more significantly than either 2-DG or UA-4 alone (Fig. 4c–4d). The analysis indicated that UA-4 alone could make cells to stay in their quiescent G0 state without an increase in size. While in combination, UA-4 and 2-DG blocked one of the two important checkpoints, namely G2/M checkpoint. As a result, the cellular DNA synthesis and mitosis could be blocked. The p53 plays an important role in controlling mechanisms at both G1/S and G2/M checkpoints.

The activation of caspase family members is essential for both death receptor and mitochondrial pathways apoptosis, these caspases are classified into two groups including initiator caspases (-2, -8, -9 and -10) and effector caspases (-3, -6 and -7) according to their functions⁴³. Our data showed that UA-4 combined with 2-DG could dose-dependently increase cell apoptosis by activating caspase-3, caspase-8 and caspase-9. The combination of 2-DG and UA-4 synergistically inhibited cancer cell growth, but it was not entirely attributed to apoptosis (Figs. 4c and 5b). The combination of 2-DG and UA-4 induced the decrease of intracellular ATP level (Fig. 5g). In lactate production assay, interestingly, UA-4 itself did not change

lactate production of the cancer cells within the effective inhibitory concentrations (2, 4, and 6 μM), but UA-4 seems to sensitize the cancer cells to the inhibitory activity of 2-DG (Fig. 5h). Moreover, the combination of 2-DG and UA-4 also synergistically inhibits tumor growth *in vivo*, compared with single drug (Fig. 6). Thus, the result indicated that the combination may target both cell necrosis/apoptosis and glycolytic pathways—a promising strategy for inhibiting cancer progression.

In conclusion, we have designed and synthesized a series of novel ursolic acid derivatives. The molecular docking model predicted that UA derivatives with different length of carbon chains (2C ~ 8C) possessed a potential for targeting glucose metabolism pathway in tumor cells. The experimental results suggest that (1) the structural modification enhanced anti-proliferative activity of UA against cancer cells; (2) the leading US597 (UA-4) significantly improved anti-cancer activity evidenced in cell cycle arrest, mitochondrial inhibition and apoptosis/necrosis induction; and (3) the combination of UA-4 and 2-DG synergistically inhibited hepatoma cancer cell growth *in vitro* and *in vivo* by inducing cell cycle arrest at G2/M stage, promoting caspase-3,8,9 activities, reducing hexokinase activity, aggravating depletion of intracellular ATP and decreasing lactate production. The combination of UA-4 and 2-DG may represent a novel strategy for cancer therapeutic treatment.

Methods

Chemicals and spectral characterization methods. UA (purity > 90%; Fig. 1) was purchased from Xi'an Ocean Biological Engineering Co., China. Silica gel (200–300 mesh) used in column chromatography was provided by Tsingtao Marine Chemistry Co., China. 3-O-acetyl-ursolic acid was prepared following the procedures described previously in detail²⁶. Other reagents at either analytical or chemical purity standards were obtained from commercial suppliers. Melting points were determined by using an electrically heated X-4 digital visual melting point apparatus. IR spectra and ¹H-NMR spectra of synthesized compounds were recorded by using a Shimadzu FTIR-8400S and a BRUKER AV-400 or AVANCE III 500 spectrometer (using TMS as the internal standard in CDCl₃ or DMSO-d₆), respectively. Electrospray ionization (ESI) mass spectra of synthesized compounds were measured by using an Agilent 1100 IC/MSD Trap XCT.

Computational modeling. To understand the molecular interaction between UA derivatives and glucokinase, a molecular docking study was carried out using the Hex 6.3 protocol⁴⁴. The crystal structure of glucokinase was used as the docking protein³⁶.

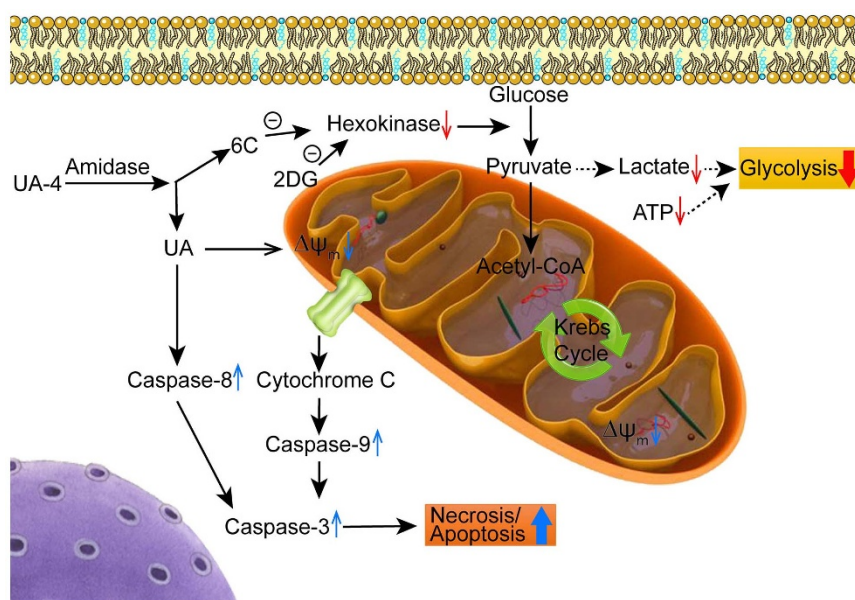


Figure 7 | Proposed mechanisms by which the leading UA derivative UA-4 and 2-DG produce synergistic inhibition on cancer cell proliferation. After entering the cells, UA-4 is hydrolyzed by amidase to be broken down to the carbon chain 6C and UA metabolite. The former competes with glucose for binding to hexokinase to inhibit cancer glycolysis pathway, while the latter produces depolarization in $\Delta\Psi_m$, cell arrest, ATP consumption, necrosis/apoptosis via caspase-independent pathway. 2-DG also inhibits glycolysis of cancer cells by targeting hexokinase. The dual targeting of cell necrosis/apoptosis and glycolysis pathways by using the safe and effective molecules represents a novel anticancer agent.



Following molecular mechanics energy minimization, the different length of carbon chain fragments (simply named as 2C, 4C, 6C and 8C, Fig. 1) of the synthesized UA derivatives UA-2 ~ UA-9 (Fig. 1) was optimized with DFT/6-31G in Gaussian 09⁴⁵ to be docked to the hexokinase homology. They were selected as the potential hexokinase inhibitor. The hexokinase structure was rigid, while the ligands 2C, 4C, 6C and 8C were flexible during the docking process. The relative binding free energy calculated with the Hex 6.3 protocol was determined as the most suitable binding orientation and the best docked structure. All parameters were calculated with the default protocols unless otherwise noted.

Chemical modification of UA derivatives. Preparation and characterization of compounds UA-2 ~ UA-5 were similar to what reported previously²⁶. Briefly, oxalyl chloride (0.6 mL) was added in three aliquots to the methylene chloride (CH₂Cl₂) solution containing compound UA-1 (1 mmol) and stirred at room temperature for 24 h. The mixture was concentrated to dryness under a reduced pressure to obtain crude 3-O-acetylsulfonyl chloride. This intermediate was dissolved in the CH₂Cl₂ (20 mL) solution, and then treated with ethylenediamine, butanediamine and hexamethylenediamine, respectively. The mixture was stirred at room temperature for 12 h, treated with triethylamine to reach pH 8–9, and concentrated to dryness. The residue was dissolved in 10 mL water, adjusted to pH 3–4 with 2 N HCl and filtered. The crude material was purified on the silica gel column with the chloroform/acetone (v/v 1:5) eluents to yield compounds UA-2 ~ UA-5, respectively.

Synthesis and characterization of UA-6 ~ UA-9 were conducted as follows: a solution of UA-2 ~ 5 in aqueous NaOH (4 N) in CH₃OH: THF (1:1.5, v:v) was stirred for 4 h at room temperature and concentrated under a reduced pressure. The residue was suspended in water, adjusted with 2 N HCl to pH 3–4 and then filtered. The filter was washed with water to pH 6–7, and the material was dried to obtain compounds UA-6 ~ UA-9.

Chromatographic analyses. UA-4 was analyzed using a reversed phase HPLC system (Waters 2695 XE, USA). The system was controlled under the following conditions: flow rate, 1.0 mL/min; column temperature, 35°C; UV detection wavelength, 210 nm. A 10 µL aliquot of UA-4 was auto-injected into the injection loop, and chromatographed using the C18 column eluted isocratically with a mobile phase of 90% methanol and 10% water. The area under each peak was calibrated with the data processor. The sample was diluted with methanol immediately before injection.

Cell lines, cell culture and mice. Human hepatocellular carcinoma HepG2 cells, gastric adenocarcinoma AGS cells, melanoma A-375 cells, cervical carcinoma HeLa cells, normal human embryonic lung fibroblast HELF cells and human liver cell line L02 cells were obtained from our in-house frozen cell stock cryopreserved in ampoules in a large repository²⁶. These cell lines were maintained in RPMI 1640 medium supplemented with heat-inactivated fetal bovine serum (FBS, 10%), penicillin (100 U/mL), and streptomycin (100 µg/mL) in a humidified atmosphere of 5.0% CO₂ at 37°C. Kunming mice, which were purchased from the Slac Animal Inc (Shanghai, China), were maintained in a controlled environment of temperature at 20°C to 25°C and 12-h cycles of light and dark. The mouse ascites hepatoma H22 cell line (Kunming background), purchased from Shanghai Cell Bank in China, was grown in DMEM supplemented with 10% FBS and 4 mM glutamine.

MTT assay for cell viability/proliferation. Ursolic acid (UA), paclitaxel, and compounds UA-1 ~ UA-9 were dissolved in dimethyl sulfoxide (DMSO) and diluted with culture medium containing 0.1% DMSO, respectively. In parallel, cells were incubated with culture medium containing 0.1% DMSO as vehicle-treated control. Paclitaxel was used as a positive control. The cytotoxicity of the derivatives was determined by the MTT assay. Cells (1 × 10⁴/well) were plated in 100 µL of the culture medium/well on 96-well plates. After overnight incubation, cells were treated with different concentrations of drugs in RPMI 1640 with 10% FBS for 24 h. After the treatment, cells were incubated with the MTT agent in the medium without phenol red and serum for another 4 h. MTT-formazan formed metabolically by viable cells was dissolved in 150 µL of DMSO and shaken for 10 min. Absorbance was then measured on an ELISA reader at the wavelength of 492 nm. Each test was repeated at least three times. The concentration of the compound which gives the 50% growth inhibition value was defined as the IC₅₀.

Cell cycle analysis. Flow cytometer method used for determining cell cycle arrest was similar to that described previously^{46–49} with minor modifications for individual analogs. Briefly, A-375 cells were incubated with different concentrations of the leading compound UA-4 (0, 1, 3 and 5 µM) for 24 h, and HepG2 cells were untreated/treated by 2-DG (20 mM), UA-4 (4 µM) and 2-DG + UA-4 (20 mM + 4 µM) for 24 h. After treatment, cells (1 × 10⁶) were harvested and washed twice with PBS, and fixed in 70% ice-cold ethanol overnight. Sample was then stained for DNA with a mixture solution of 1% (v/v) Triton X-100, 0.01% RNase, and 0.05% PI for 30 min at 4°C in the dark. Cell cycle distribution was then determined by using flow cytometry (BD Bioscience, FACS AriaIII). All experiments were performed three times.

Mitochondrial membrane potential assay. The mitochondrial membrane potential (ΔΨ_m) assay was similar to that described previously^{50,51}. The assay is based on uptake of 2-(6-Amino-3-imino-3H-xanthen-9-yl)-benzoic acid methyl ester (Rhodamine 123, inhibitor of mitochondrial oxidative phosphorylation) by mitochondria. Increased uptake of Rhodamine 123 indicates loss of ΔΨ_m. Briefly,

A-375 cells were cultured on 6-well plates overnight and then incubated with UA-4 (1, 5 and 10 µM) in 3 mL fresh culture medium. Cells were then incubated for 24 h. Cells were washed twice with PBS and incubated with Rhodamine 123 for 10 min. The percentage of Rhodamine-positive cells was determined by using flow cytometry (BD Bioscience, FACS AriaIII).

Analysis of distinction between apoptotic and necrotic cells. For distinguishing apoptotic and necrotic cells, the treated cells were stained with Annexin V-FITC and propidium iodide (PI) double staining kit. A-375 or HepG2 cells were incubated with different concentrations of UA-4 and/or 2-DG, 2-DG + UA-4 for 24 h. After the treatment, 3 × 10⁵ cells were harvested and washed twice with PBS and stained with 5 µL of the solution containing Annexin V-FITC and PI for 15 min in the dark according to the manufacturer's instructions. Cells were then analyzed by using flow cytometry (BD Bioscience, FACS AriaIII). All experiments were performed three times.

TdT-UTP nick end labeling (TUNEL) assays were performed with the one step TUNEL kit according to the manufacturer's instructions (Biyotime, China). Briefly, the cells were fixed with 4% paraformaldehyde buffer saline, rinsed with PBS, treated with 0.1% Triton X-100 for 2 min on ice, incubated with TUNEL for 1 h at 37°C. The FITC-labeled TUNEL-positive cells were analyzed by flow cytometry. The TUNEL-positive cells were recognized as apoptotic cells.

Assessment of synergism between UA-4 and 2-DG. To examine if a synergistic effect existed between UA-4 and glycolytic inhibitors (such as L-cysteine (L-Cys), 2-DG, levanisole (LM) and 3-bromopyruvate (3-BrPA)), cancer cells cultured on 96-well plates were treated with UA-4 (4 µM) and the combination of glycolytic inhibitor (IC₈₀) and UA-4 (4 µM), respectively, for 24 h. For the combination of 2-DG and UA-4, each cell line was divided into the following four groups, and treated differently with different concentrations of either 2-DG, UA-4, or the combination: (1) vehicle-treated control group; (2) 2-DG group (10, 20 and 40 mM); (3) UA-4 group (2, 4 and 6 µM); (4) 2-DG (mM) + UA-4 (µM) group (10 + 2, 20 + 4 and 40 + 6). The cell viability was determined by the MTT assay. Parallel experiments were performed in A-375 (cancer), HELF (normal), HepG2 (cancer) and L02 (normal) cell lines for three times.

Quantification of caspase -3, -8, -9 activity. The working principles of Caspase-3, -8 or -9 Activity Assay Kit (Biyotime, China) are based on the cleavage of the following substrate: acetyl-Asp-Glu-Val-Asp *p*-nitroanilide (Ac-DEVD-pNA), acetyl-Ile-Glu-Thr-Asp *p*-nitroanilide (Ac-IETD-pNA) and acetyl-Leu-Glu-His-Asp *p*-nitroanilide (Ac-LEHD-pNA). Lysates of HepG2 cells were prepared after treating with 2-DG (0, 10, 20 mM), UA-4 (0, 2, 4 µM) and 2-DG + UA-4 (0, 10 + 2, 20 + 4) for 24 h. Lysates were incubated at 37°C for 4 h. Samples were measured with a microplate reader (Tecan Infinite® 200 PRO, Switzerland) at an absorbance of 405 nm⁵². The concentration of *p*-nitroaniline (pNA) is proportional to caspase activity and normalized to protein concentration.

Hexokinase activity assay. Cellular hexokinase (HK) activity levels were measured with a Hexokinase Activity Assay Kit obtained from Keming (Keming Biotechnology Co., Ltd, China). HepG2 cells were seeded in a 6-well culture plate, treated with 2-DG (0, 10, 20 mM), UA-4 (0, 2, 4 µM) and 2-DG + UA-4 (0, 10 + 2, 20 + 4) for 24 h. Protein concentrations of cell lysates were measured, and glycolytic enzyme activities were evaluated. HK activity was assayed at 37°C for 5 min in basic medium containing 50 mM Tris-HCl (pH 7.4), 5 mM MgCl₂, 1 mM glucose, 1 mM ATP, 0.2 mM NAD⁺ and 1 U/mL glucose-6-phosphate dehydrogenase at 340 nm.

Measurements of intracellular ATP. The ATP level was measured using a luciferase-luciferin ATP Assay Kit (Beyotime, China) following the manufacturer's instructions. Briefly, HepG2 cells were seeded in 6-well plates at a density of 3 × 10⁵ cells per well and cultivated for 24 h. After 12-h incubation with 2-DG (0, 10, 20, 40 mM), UA-4 (0, 2, 4, 6 µM) and 2-DG + UA-4 (0, 10 + 2, 20 + 4, 40 + 6), cells were washed twice with PBS and then resolved with ATP lysis buffer on ice. ATP in cell lysate was measured using a microplate reader (Tecan Infinite® 200 PRO, Switzerland), and the ATP concentration was normalized to protein concentration. The ATP level (%) = mean ATP concentration of treated group/mean ATP concentration of control group × 100%.

Lactate production assay. Lactate was measured in cell culture supernatants by use of the Lactate Assay Kit (KeyGEN, Nanjing, China). Briefly, HepG2 cells (3 × 10⁵/well) were treated with 2-DG (0, 10, 20, 40 mM), UA-4 (0, 2, 4, 6 µM) and 2-DG + UA-4 (0, 10 + 2, 20 + 4, 40 + 6) for 24 h. Optical density (OD) was measured at 530 nm, and the lactate concentration was normalized for number of cells. Results are presented as means ± SD from triplicate wells after subtracting the background for culture medium.

Theoretical analysis of the interaction between UA-4 and 2-DG. To analyze the interaction between UA-4 and 2-DG, calculation method of Zheng-Jun Jin³⁹ was used. This method provides a “q” value, according to which the interaction between two drugs can be classified as antagonistic effect (q ≤ 0.85), additive effect (0.85 < q < 1.15) or synergistic effect (q ≥ 1.15). And the formula is q = E_{A+B} / (E_A + E_B - E_A * E_B), where E_{A+B}, E_A and E_B are average inhibiting effect of combination treatment, effect of drug A only and effect of drug B only, respectively.



Animal experiments. All animals used in these investigations were handled in accordance with the Guide for the Care and Use of Laboratory Animals (National Research Council, 1996). The institutional animal care and use committee of Fuzhou University reviewed and approved all animal use procedures based on the above regulations, including use of appropriate species, quality and number of animals, avoidance or minimization of discomfort, distress and pain of animals in concert with sound science, use of appropriate anaesthesia and euthanasia. All possible efforts were made to minimize the animals' suffering and to reduce the number of animals used.

H22 cells (2×10^7 cells in 200 μ L of mice ascites) were injected subcutaneously into the right hind leg of 8-week-old female Kunming mice. Two days after injection of cells, the mice were imaged to verify tumor establishment. A total of 36 Kunming mice were equally divided into six groups randomly, and then they were orally gavaged with either normal saline (control), 2-DG (1 g/Kg), UA-4 (40 mg/Kg), UA-4 (80 mg/Kg), 2DG + UA-4 (1 g/Kg + 40 mg/Kg) or 2-DG + UA-4 (1 g/Kg + 80 mg/Kg) for 14 days, respectively. Mice weight and tumor volume were measured every other day, and tumour volume was estimated using the formula for an ellipsoid ($0.5 \times \text{length} \times \text{width}^2$). After 14 days of treatment, the mice were sacrificed by cervical dislocation after euthanizing with isoflurane (3%), and tumor volume and weight were measured, and fixed in formalin. These tumors were then paraffin embedded and stained with hematoxylin and eosin (H&E). Tumor inhibition rate (%) = (mean tumor weight of control group - mean tumor weight of treated group)/mean tumor weight of control group $\times 100\%$.

Statistical analysis. Data represented the means \pm standard deviations (SD) for three independent experiments. Significance of differences between experimental variables was determined by Student's t-test and one-way analysis of variance. Multiple comparisons of means were conducted using the least significance difference (LSD) test. A probability (P) value < 0.05 was considered statistically significant, and $P < 0.01$ was highly statistical significance. All statistical analyses were performed employing the SPSS statistical software (version 19.0).

- Chattopadhyay, D. *et al.* Antimicrobial and anti-inflammatory activity of folklore: *Mallotus peltatus* leaf extract. *J Ethnopharmacol.* **82**, 229–237 (2002).
- Lu, J. *et al.* Ursolic acid improves high fat diet-induced cognitive impairments by blocking endoplasmic reticulum stress and I κ B kinase β /nuclear factor- κ B-mediated inflammatory pathways in mice. *Brain Behav Immun.* **25**, 1658–1667 (2011).
- Shanmugam, M. K. *et al.* Ursolic acid inhibits the initiation, progression of prostate cancer and prolongs the survival of TRAMP mice by modulating pro-inflammatory pathways. *Plos One* **7**, e32476 (2012).
- Lee, J. *et al.* Ursolic acid ameliorates thymic atrophy and hyperglycemia in streptozotocin–nicotinamide-induced diabetic mice. *Chem-Biol Interact.* **188**, 635–642 (2010).
- Kunkel, S. D. *et al.* Ursolic Acid Increases Skeletal Muscle and Brown Fat and Decreases Diet-Induced Obesity, Glucose Intolerance and Fatty Liver Disease. *Plos One* **7**, e39332 (2012).
- Ma, C. *et al.* Inhibitory Effects on HIV-1 Protease of Constituents from the Wood of *Xanthoceras s orbifolia*. *J Nat Prod.* **63**, 238–242 (2000).
- Kashiwada, Y. *et al.* Anti-AIDS Agents 38. Anti-HIV Activity of 3-O-Acyl Ursolic Acid Derivatives. *J Nat Prod.* **63**, 1619–1622 (2000).
- Baglin, I. *et al.* A review of natural and modified betulinic, ursolic and echinocystic acid derivatives as potential antitumor and anti-HIV agents. *Mini Rev Med Chem.* **3**, 525–539 (2003).
- Huang, L., Yu, D., Ho, P., Lee, K. H. & Chen, C. H. Synthesis and anti-HIV activity of bi-functional triterpene derivatives. *Lett Drug Des Discov.* **4**, 471–478 (2007).
- Wang, Z., Hsu, C. & Yin, M. Antioxidative characteristics of aqueous and ethanol extracts of glossy privet fruit. *Food Chem.* **112**, 914–918 (2009).
- Mullié, C., Jonet, A., Dassonville-Klimpt, A., Gosmann, G. & Sonnet, P. Inhibitory effect of ursolic acid derivatives on hydrogen peroxide- and glutathione-mediated degradation of hemin: A possible additional mechanism of action for antimalarial activity. *Exp Parasitol.* **125**, 202–207 (2010).
- Yan, S., Huang, C., Wu, S. & Yin, M. Oleanolic acid and ursolic acid induce apoptosis in four human liver cancer cell lines. *Toxicol in Vitro.* **24**, 842–848 (2010).
- Tang, C. *et al.* Downregulation of survivin and activation of caspase-3 through the PI3K/Akt pathway in ursolic acid-induced HepG2 cell apoptosis. *Anti-Cancer Drug.* **20**, 249–258 (2009).
- Andersson, D., Cheng, Y. J. & Duan, R. D. Ursolic acid inhibits the formation of aberrant crypt foci and affects colonic sphingomyelin hydrolyzing enzymes in azoxymethane-treated rats. *J Cancer Res Clin.* **134**, 101–107 (2008).
- Huang, C. Y., Lin, C. Y., Tsai, C. W. & Yin, M. C. Inhibition of cell proliferation, invasion and migration by ursolic acid in human lung cancer cell lines. *Toxicol in Vitro.* **25**, 1274–1280 (2011).
- Hsu, Y. L., Kuo, P. L. & Lin, C. C. Proliferative inhibition, cell-cycle dysregulation, and induction of apoptosis by ursolic acid in human non-small cell lung cancer A549 cells. *Life Sci.* **75**, 2303–2316 (2004).
- Sporn, M. B. & Suh, N. Chemoprevention of cancer. *Carcinogenesis* **21**, 525–530 (2000).
- Chen, L., Qiu, W., Tang, J., Wang, Z. F. & He, S. Y. Synthesis and bioactivity of novel nitric oxide-releasing ursolic acid derivatives. *Chinese Chem Lett.* **22**, 413–416 (2011).
- Meng, Y. Q. *et al.* The synthesis of ursolic acid derivatives with cytotoxic activity and the investigation of their preliminary mechanism of action. *Bioorgan Med Chem.* **17**, 848–854 (2009).
- Chadalapaka, G., Jutooru, I., McAlees, A., Stefanac, T. & Safe, S. Structure-dependent inhibition of bladder and pancreatic cancer cell growth by 2-substituted glycyrrhetic and ursolic acid derivatives. *Bioorg Med Chem Lett.* **18**, 2633–2639 (2008).
- Kazakova, O. B., Giniyatullina, G. V., Yamansarov, E. Y. & Tolstikov, G. A. Betulin and ursolic acid synthetic derivatives as inhibitors of Papilloma virus. *Bioorg Med Chem Lett.* **20**, 4088–4090 (2010).
- Liu, D., Meng, Y. Q., Zhao, J. & Chen, L. G. Synthesis and anti-tumor activity of novel amide derivatives of ursolic acid. *Chem Res Chinese U.* **24**, 42–46 (2008).
- Quan, P. *et al.* The effects of water-soluble polymers on hydroxypropyl-beta-cyclodextrin solubilization of oleanolic acid and ursolic acid. *J Incl Phenom Macro.* **63**, 181–188 (2009).
- Gnoatto, S. C. B. *et al.* Pharmacomodulation on the 3-acetylursolic acid skeleton: Design, synthesis, and biological evaluation of novel N-[3-[4-(3-aminopropyl) piperazinyl] propyl]-3-O-acetylursolamide derivatives as antimalarial agents. *Bioorgan Med Chem.* **16**, 771–782 (2008).
- Gnoatto, S. C. B. *et al.* Evaluation of ursolic acid isolated from *Ilex paraguariensis* and derivatives on aromatase inhibition. *Eur J Med Chem.* **43**, 1865–1877 (2008).
- Shao, J. W. *et al.* In vitro and in vivo anticancer activity evaluation of ursolic acid derivatives. *Eur J Med Chem.* **46**, 2652–2661 (2011).
- Dang, C. V., Hamaker, M., Sun, P., Le, A. & Gao, P. Therapeutic targeting of cancer cell metabolism. *J Mol Med.* **89**, 205–212 (2011).
- Warburg, O., Wind, F. & Negelein, E. The metabolism of tumors in the body. *J Gen Physiol.* **8**, 519–530 (1927).
- Vander Heiden, M. G. Targeting cancer metabolism: a therapeutic window opens. *Nat Rev Drug Discov.* **10**, 671–684 (2011).
- Zhong, D. *et al.* The glycolytic inhibitor 2-deoxyglucose activates multiple prosurvival pathways through IGF1R. *J Biol Chem.* **284**, 23225–23233 (2009).
- Cheng, G. *et al.* Mitochondria-targeted drugs synergize with 2-deoxyglucose to trigger breast cancer cell death. *Cancer Res.* **72**, 2634–2644 (2012).
- Xi, H. *et al.* 2-Deoxy-D-glucose activates autophagy via endoplasmic reticulum stress rather than ATP depletion. *Cancer Chemoth Pharm.* **67**, 899–910 (2011).
- Kang, H. T. & Hwang, E. S. 2-Deoxyglucose: an anticancer and antiviral therapeutic, but not any more a low glucose mimetic. *Life Sci.* **78**, 1392–1399 (2006).
- Raez, L. E. *et al.* A phase I dose-escalation trial of 2-deoxy-d-glucose alone or combined with docetaxel in patients with advanced solid tumors. *Cancer Chemoth Pharm.* **71**, 523–530 (2013).
- Maschek, G. *et al.* 2-deoxy-D-glucose increases the efficacy of adriamycin and paclitaxel in human osteosarcoma and non-small cell lung cancers in vivo. *Cancer Res.* **64**, 31–34 (2004).
- Kamata, K., Mitsuya, M., Nishimura, T., Eiki, J. & Nagata, Y. Structural basis for allosteric regulation of the monomeric allosteric enzyme human glucokinase. *Structure.* **12**, 429–438 (2004).
- Agius, L. & Stubbs, M. Investigation of the mechanism by which glucose analogues cause translocation of glucokinase in hepatocytes: evidence for two glucose binding sites. *Biochem J.* **346**, 413–421 (2000).
- Ikuta, K. *et al.* Defects in apoptotic signal transduction in cisplatin-resistant non-small cell lung cancer cells. *Oncol Rep.* **13**, 1229–1234 (2005).
- Sha, J. *et al.* Synergistic effect and mechanism of vitamin A and vitamin D on inducing apoptosis of prostate cancer cells. *Mol Biol Rep.* **40**, 2763–2768 (2013).
- Ramírez-Peinado, S. *et al.* 2-deoxyglucose induces Noxa-dependent apoptosis in alveolar rhabdomyosarcoma. *Cancer Res.* **71**, 6796–6806 (2011).
- Goldberg, L., Israeli, R. & Kloog, Y. FTS and 2-DG induce pancreatic cancer cell death and tumor shrinkage in mice. *Cell Death Dis.* **3**, e284 (2012).
- Aghae, F., Islamian, J. P. & Baradaran, B. Enhanced radiosensitivity and chemosensitivity of breast cancer cells by 2-deoxy-d-glucose in combination therapy. *J Breast Cancer.* **15**, 141–147 (2012).
- Muñoz-Pinedo, C. [Signaling Pathways that Regulate Life and Cell Death: Evolution of Apoptosis in the Context of Self-Defense]. *Self and Nonself* [López-Larrea, C. (ed.)] [124–143] (Springer, New York, 2012).
- Macindoe, G., Mavridis, L., Venkatraman, V., Devignes, M. D. & Ritchie, D. W. HexServer: an FFT-based protein docking server powered by graphics processors. *Nucleic Acids Res.* **38**, W445–449 (2010).
- Frisch, M. J. *et al.* Gaussian 09, Revision A.1. (Gaussian, Inc. Wallingford CT, 2009).
- Shao, J. *et al.* Synthesis and antitumor activity of emodin quaternary ammonium salt derivatives. *Eur J Med Chem.* **56**, 308–319 (2012).
- Wang, W. *et al.* Synthesis and biological activity evaluation of emodin quaternary ammonium salt derivatives as potential anticancer agents. *Eur J Med Chem.* **56**, 320–331 (2012).
- Wang, J. *et al.* Synthesis, Spectral Characterization, and In Vitro Cellular Activities of Metapristone, a Potential Cancer Metastatic Chemopreventive Agent Derived from Mifepristone (RU486). *AAPS J.* **16**, 289–298 (2014).
- Lu, Y. *et al.* Nitric Oxide Inhibits Hetero-adhesion of Cancer Cells to Endothelial Cells: Restraining Circulating Tumor Cells from Initiating Metastatic Cascade. *Scientific Rep.* **4**, 1–9 (2014).



50. Shao, J. *et al.* Intracellular distribution and mechanisms of actions of photosensitizer Zinc (II)-phthalocyanine solubilized in Cremophor EL against human hepatocellular carcinoma HepG2 cells. *Cancer Lett.* **330**, 49–56 (2012).
51. Shao, J. *et al.* Inhibition of human hepatocellular carcinoma HepG2 by phthalocyanine photosensitizer PHOTOCYANINE: ROS production, apoptosis, cell cycle arrest. *Eur J Cancer.* **48**, 2086–2096 (2012).
52. Yuan, S. *et al.* Voltage-dependent anion channel 1 is involved in endostatin-induced endothelial cell apoptosis. *FASEB J.* **22**, 2809–2820 (2008).

Acknowledgments

This research was supported by the National Science Foundation of China (No. 81201709 and No. 81273548), the National Science Foundation for Fostering Talents in Basic Research of China (No. J1103303), the Foundation of the Education Department of Fujian Province, China (JK2010003), the Scientific and Technological Foundation of Fujian Province of China (2011J0104) and the China Postdoctoral Science Foundation (No.2012M511441 and No. 2013T60638). The funders had no role in study design, data collection and analysis, decision to publish, or preparation of the manuscript.

Author contributions

J.W. and Z.J.: manuscript writing, development of methodology, acquisition of data, analysis and interpretation of data; Y.L., L.X., M.O., Y.L., L.L. and X.Y.: acquisition of data

and figures; J.C. and Y.D.: technical support; J.S. and L.J.: conception and design, study supervision, review and/or revision of the manuscript.

Additional information

Supplementary information accompanies this paper at <http://www.nature.com/scientificreports>

Competing financial interests: The authors declare no competing financial interests.

How to cite this article: Wang, J.C. *et al.* Synergism of ursolic acid derivative US597 with 2-deoxy-D-glucose to preferentially induce tumor cell death by dual-targeting of apoptosis and glycolysis. *Sci. Rep.* **4**, 5006; DOI:10.1038/srep05006 (2014).



This work is licensed under a Creative Commons Attribution-NonCommercial-NoDerivs 3.0 Unported License. The images in this article are included in the article's Creative Commons license, unless indicated otherwise in the image credit; if the image is not included under the Creative Commons license, users will need to obtain permission from the license holder in order to reproduce the image. To view a copy of this license, visit <http://creativecommons.org/licenses/by-nc-nd/3.0/>